Albahit Journal of Applied Sciences
"open-access, peer-reviewed biannual journal"
eISSN: 2708-8936, pISSN: 2708-244X
Volume 5, Issue 1, 2026
Page No: 75-86
Website: *https://albahitjas.com.ly/index.php/albahit/en/index*

Impact of peripheral ligand modification on MLCT stability and optical properties of Ru(II) complexes for potential photocatalytic application

Hadeel Ali Mohammed [1*], Hamid. M. Younis [2]
[1,2] Chemistry Department, Faculty of Science, Sirte University, Sirte-Libya.
[*]*Corresponding author:* hadeel-alsed@su.edu.ly

Received: 14-10-2025	**Accepted:** 27-12-2025	**Published:** 15-01-2026

Abstract:
This study investigates the role of peripheral ligand modification in controlling the MLCT energetics and photochemical stability of Ru(II) polypyridyl complexes, using tbbpy- and dppz-based systems as a comparative platform. By combining ^{1}H NMR spectroscopy, steady-state UV–Vis absorption, and time-dependent photochemical kinetics, we demonstrate that peripheral ligands act as electronically active components rather than passive structural substituents.
A key finding of this work is the spectral invariance of the Ru–tbbpy complex in both aprotic (CH_3CN) and protic (CH_3OH) solvents, which provides a rare baseline for isolating solvent-driven photochemical pathways. In contrast, incorporation of the π-extended dppz ligand induces a systematic increase in the MLCT energy gap and markedly enhances photochemical robustness under continuous irradiation. Kinetic analysis in methanol reveals pseudo-first-order behavior for the tbbpy system, with an apparent rate constant of $(3.3 \pm 0.2) \times 10^{-3}$ min^{-1} and a half-life of approximately 210 min.
The emergence of new ligand-centered absorption bands upon irradiation indicates photo-induced transformation into stable photoproducts rather than nonspecific decomposition. These results highlight peripheral ligand design as an effective strategy for modulating MLCT stability and improving the durability of Ru(II)-based photosensitizers, offering mechanistic insights relevant to the rational development of photoactive coordination complexes.

Keywords: Ru(II) complexes, Photochemical degradation ,tbbpy and dppz ligands, pseudo-first-order kinetics, Apparent rate constant, solvent effects, MLCT.

تأثير تعديل الروابط الطرفية على استقرار نقل الشحنة من المعدن إلى الرابطة (*MLCT*) والخواص البصرية لمركبات الروثينيوم (*II*) لتطبيقات التحفيز الضوئي المحتملة

هديل علي محمد [1*]، حامد محمد يونس [2]
[2،1] قسم الكيمياء، كلية العلوم، جامعة سرت، سرت، ليبيا

الملخص
تبحث هذه الدراسة دور تعديل الروابط الطرفية في التحكم بطاقة نقل الشحنة من المعدن إلى الرابطة (MLCT) والاستقرار الكيميائي الضوئي لمركبات الروثينيوم (II) متعددة البيريديل، باستخدام أنظمة tbbpy و dppzكمنصة مقارنة. من خلال الجمع بين مطيافية الرنين النووي المغناطيسي للبروتون(^{1}H NMR) ، وامتصاص الأشعة فوق البنفسجية والمرئية في الحالة المستقرة، والحركية الكيميائية الضوئية المعتمدة على الزمن، نُبين أن الروابط الطرفية تعمل كمكونات نشطة إلكترونيًا وليست بدائل هيكلية خاملة.
تُبين هذه الدراسة أن الروابط الطرفية تعمل كمكونات نشطة إلكترونيًا وليست بدائل هيكلية خاملة. من أهم نتائج هذا العمل ثبات الطيف لمركب Ru–tbbpy في كل من المذيبات غير البروتونية (CH_3CN) والبروتونية(CH_3OH) ، مما يوفر أساسًا نادرًا لعزل المسارات الكيميائية الضوئية التي يحركها المذيب. في المقابل، يؤدي إدخال رابطة dppz الممتدة π إلى زيادة منتظمة في فجوة طاقة MLCT ويعزز بشكل ملحوظ الثبات الكيميائي الضوئي تحت الإشعاع المستمر. يكشف التحليل الحركي في الميثانول عن سلوك من الرتبة الأولى الزائفة لنظامtbbpy ، بثابت معدل ظاهري قدره $(3.3 \pm 0.2) \times 10^{-3}$ دقيقة$^{-1}$ ونصف عمر يبلغ حوالي 210 دقيقة.
يشير ظهور نطاقات امتصاص جديدة متمركزة حول الرابطة عند الإشعاع إلى تحول ضوئي إلى نواتج ضوئية مستقرة بدلاً من التحلل غير المحدد. تُبرز هذه النتائج تصميم الروابط الطرفية كاستراتيجية فعّالة لتعديل استقرار نقل الشحنة من المعدن إلى الرابطة (MLCT) وتحسين متانة المحسسات الضوئية القائمة على الروثينيوم(II) ، مما يُقدّم رؤى آلية ذات صلة بالتطوير العقلاني لمركبات التنسيق الضوئية النشطة.

الكلمات المفتاحية: مركبات الروثينيوم (II)، التحلل الكيميائي الضوئي، روابط tbbpy وdppz، حركية التفاعل من الرتبة الأولى الزائفة، ثابت معدل التفاعل الظاهري، تأثيرات المذيب، نقل الشحنة من المعدن إلى الرابطة (MLCT).

1.Introduction

The design of effective photosensitizers utilizing Ru(II) polypyridine complexes has attracted considerable attention owing to their exceptional photophysical characteristics and chemical stability. (Fennes et al., 2024)

A significant challenge in employing these complexes is comprehending the impact of structural modifications and environmental factors, including solvent interactions, on their electronic transitions and photochemical stability. (Sun et al., 2010)

While the coordination environment of Ru(II) has been extensively studied, a more detailed investigation into the role of peripheral ligand modification is essential for the purpose of optimizing energy gaps and enhancing photostability (Sun et al., 2010; Lanquist et al., 2023). Expanding upon our previous research concerning the influence of various solvents on the spectroscopic characteristics of these systems, a more in-depth examination of the interplay between ligand structure and solvent type is warranted . (Mohammed & Younis, 2025)

The primary mechanism that dictates the behavior of these complexes is photo-excitation. As depicted in Figure 1, the absorption of visible light triggers a Metal-to-Ligand Charge Transfer (MLCT) event, wherein an electron is elevated from the metal-centered d-orbitals to the ligand-based π^* orbitals. This excitation results in a transient state whose stability and relaxation pathways are particularly sensitive to the electronic characteristics of the peripheral ligands and the surrounding solvent environment. (Suneesh et al., 2014;Di Pietro et al., 2021; Cotic et al.,2024)

In this study, we investigate the electronic properties and photochemical stability of two Ru(II) complexes featuring different peripheral ligands (tbbpy and dppz). By employing UV-Vis spectroscopy and kinetic analysis, we aim to elucidate how ligand π-extension and solvent nature dictate the degradation pathways and the overall integrity of the MLCT states, rather than focusing on catalytic turnover.

Previous work has shown that solvent environment significantly modulates the spectroscopic and photochemical properties of Ru(II) polypyridyl complexes, affecting excited-state behavior and stability (Mohammed & Younis, 2025).

Additionally, strategies that influence the interaction of Ru(II) chromophores with their surroundings can alter their photostability under prolonged irradiation (Khanduja et al., 2023).

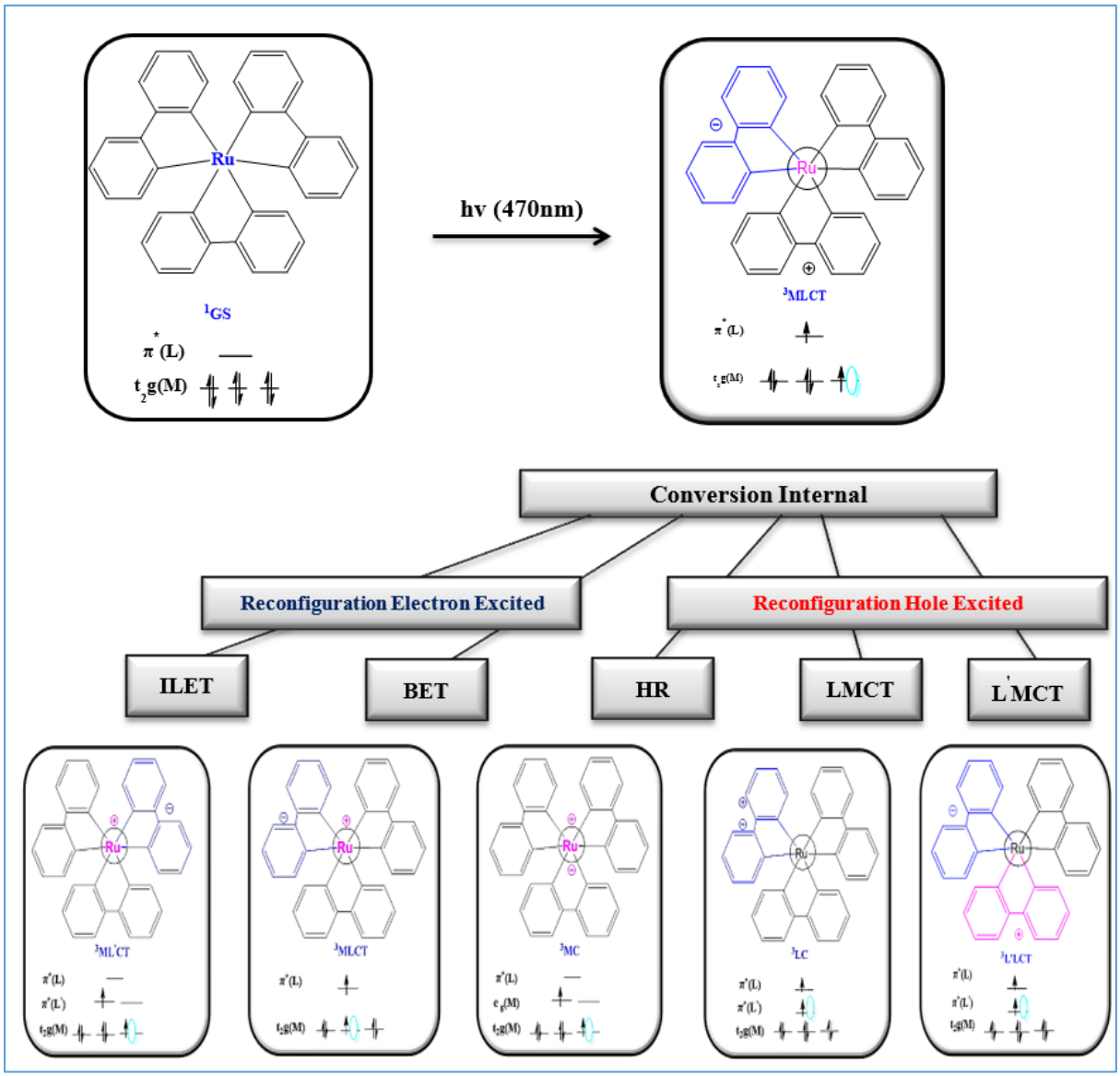

Figure 1 . Comprehensive excited-state landscape of Ru(II) polypyridine complexes following photoexcitation(Cotic et al.,2024).

2. Experimental

2.1 Materials and methods

The Ru(II) complexes investigated in this study were prepared following the methodology described by Sven Rau et al. (Scheme 1). The Chem Draw scheme emphasizes the central $Ru(bpy)_2$ core and the differing peripheral ligands. All spectroscopic analyses, including UV–Vis measurements, were conducted on the complexes prepared as described.

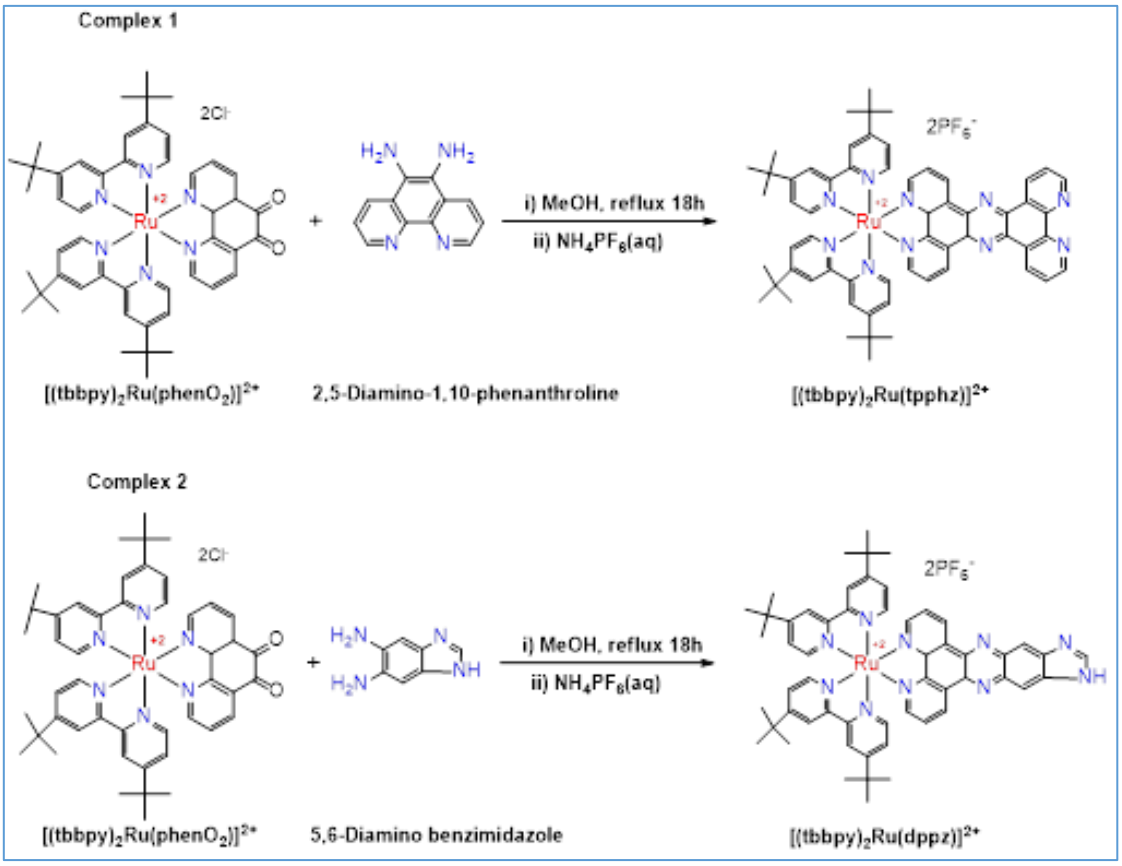

Figure 2. Structures of the Ru(II) complexes examined, illustrating the central Ru(bpy)$_2$ core and the varying peripheral ligands. (Bolger et al., 1995; Ruslanova et al., 2002 ;Kuhnt et al., 2010).

2.2 Photochemical Study

Photochemical investigations were carried out at ambient temperature using air-equilibrated solutions in a 1 cm quartz cuvettes. The samples were irradiated with a 10 W blue light-emitting diode (LED) source operating at 470 nm. The emitted light closely matches the solar spectrum in terms of energy distribution. The LED employed in this study was a type A2022-110-BLUE.

2.3 Sample Preparation for Photolysis

Each sample was used as received, without further purification. All measurements were performed in air, unless stated differently. Sample solutions were made in the absence of ambient light, wrapped with aluminum foil, and tightly sealed to reduce light exposure and evaporation. Samples were produced immediately before measurements. Complexes were synthesized in acetonitrile and methanol at an approximately concentration of 1×10^{-4}M .

To ensure complete dissolution and superior homogeneity of the complexes in various solvents, an ultrasonic bath (Bandelin electronic KG, Germany) was utilized. This process also served to degas the solutions prior to spectroscopic measurements, ensuring highly accurate and reproducible data with an RSD of less than 3%.

3. Results

3.1 Ligand – dependent ^{1}H NMR proton behavior of peripheral diimine ligands

The ^{1}H NMR spectra reveal well-defined aromatic proton resonances corresponding to the terminal ligands in the investigated systems. The ^{1}H NMR data of complexes containing peripheral tbbpy ligands were originally reported in the author's master's thesis, where they

were primarily employed for structural confirmation rather than for an in-depth analysis of peripheral ligand effects. (Mohammed & Younis, 2025)

In that earlier work, a ligand-focused interpretation at the individual proton level was not undertaken. In the present study, these data are revisited and selectively summarized to enable a direct comparison with peripheral ligands of distinct electronic character.

In the tbbpy-based systems, the aromatic proton signals of the terminal ligand are confined to a relatively narrow chemical shift range. Specifically, the H^3 and H^5 protons resonate at δ = 7.8–8.2 ppm, while the nitrogen-adjacent proton H^6 appears further downfield at δ = 8.4–8.6 ppm. These resonances are sharp, well resolved, and display splitting patterns consistent with intraligand coupling.

A detailed summary of chemical shifts, multiplicities, and proton assignments for the peripheral tbbpy ligand is provided in Table 1, while a more comprehensive set of experimental conditions and extended ^1H NMR assignments are discussed in detail in the author's master's thesis. (Mohammed & Younis, 2025)

Table 1. Diagnostic ^1H NMR protons of the peripheral tbbpy ligand.

Proton	δ (ppm)	Multiplicity	J (Hz)	Integration	Relevance to peripheral ligand
H^3	7.85	d	5.6	1H	Aromatic proton sensitive to electronic distribution
H^5	8.10	d	5.6	1H	Symmetry-related aromatic proton
H^6	8.48	d	8.2	1H	N-adjacent proton, strongest deshielding
H^4	7.9–8.2	m	n .r	1H	Partially overlapped, ligand backbone

Notes: Only peripheral ligand protons directly involved in electronic modulation are reported. *(n.r* =not resolved due to overlap).

For comparative purposes, the ^1H NMR spectrum of **complex 2** bearing a terminal dppz ligand was recorded within the same collaborative research group and is provided exclusively as Supporting Information (Figure 3) .

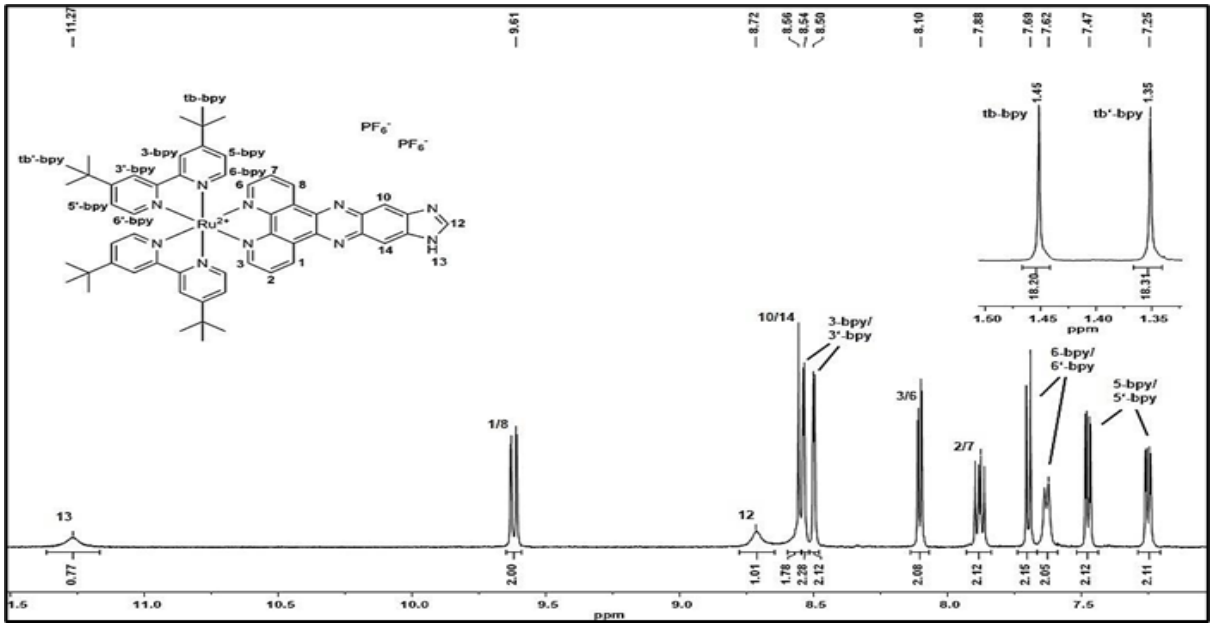

Figure 3 .[1]H NMR spectrum (400 MHz) of complex 2 bearing a terminal dppz ligand recorded in CD_3CN at 298 K. (Isakov et al., 2019)

The spectrum shows a broader distribution of aromatic resonances compared to bipyridine-type terminal ligands, spanning the δ 8.0–9.2 ppm region. The most downfield resonances (δ 8.8–9.2 ppm) are assigned to protons adjacent to the phenazine nitrogen atoms, while the remaining aromatic protons appear between δ 8.0 and 8.8 ppm ; detailed chemical shift th assignments are summarized in Table 2.

Table 2. Diagnostic [1]H NMR protons of the peripheral dppz ligand in complex 2

Proton	δ (ppm)	Multiplicity	J (Hz)	Integration	Relevance to terminal ligand
H^2	8.12	d	6.1	1H	Peripheral aromatic proton
H^3	8.46	d	6.1	1H	Fused ring proton
H^5	8.75	d	8.4	1H	N-adjacent proton
H^6	9.05	d	8.4	1H	Most deshielded N-adjacent proton

Notes: Reported protons represent the most sensitive positions to π-extension and nitrogen proximity in the peripheral dppz ligand.

3.2 Effect of peripheral ligand on UV-Vis absorption properties of Ru(II) complexes

The UV–Vis absorption maxima (λ_{max}) and corresponding energy gaps (ΔE) for Ru–tbbpy and Ru–dppz complexes in CH_3CN and CH_3OH are presented in Figure 4.

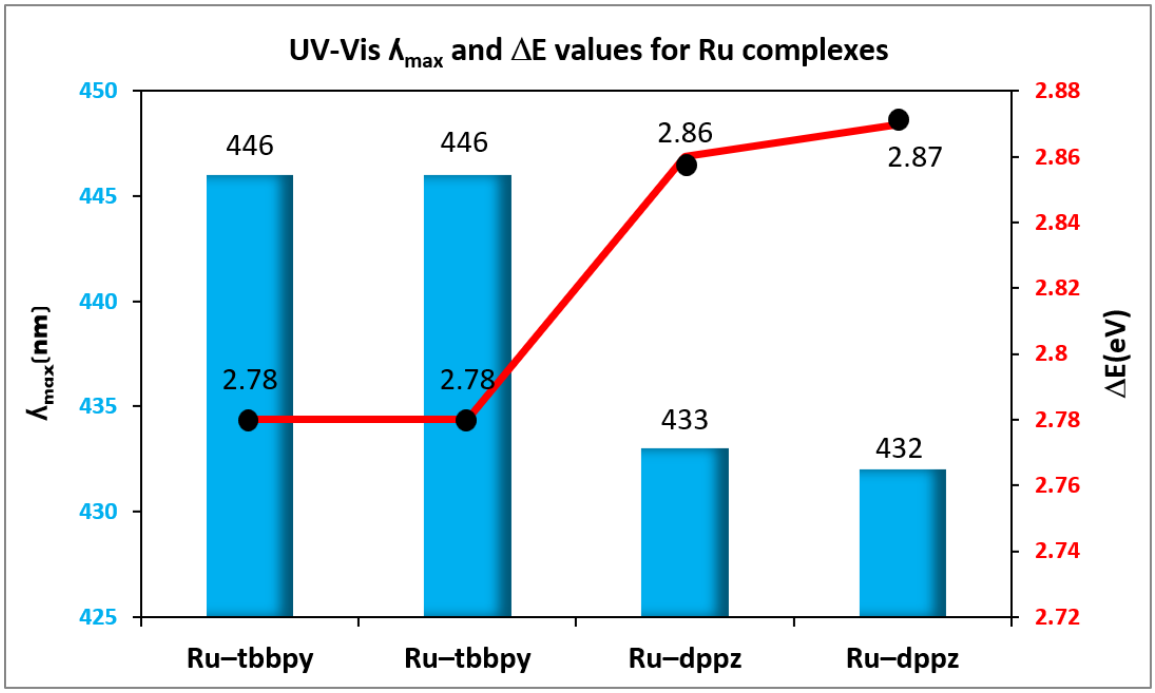

Figure 4. UV–Vis absorption maxima (λ_{max}, nm ; blue bars) and corresponding optical band gaps (ΔE, eV; red line with markers) for Ru–tbbpy and Ru–dppz complexes measured in CH_3CN and CH_3OH. The numerical values of and ΔE are indicated above each bar and data point.

Ru–tbbpy exhibits MLCT absorption bands at λ ≈ 446 nm with an optical band gap of ΔE ≈ 2.78 eV in both solvents, indicating minimal solvent dependence. In contrast, Ru–dppz displays

blue-shifted MLCT bands at λ ≈ 432–433 nm accompanied by larger band gaps (ΔE ≈ 2.86–2.87 eV).
These difference reflect the stronger π-acceptor character and extended conjugation of the dppz ligand, which stabilized the ligand-centered orbitals and leads to higher MLCT transition energies. Overall, the figure provides a clear comparison of the ligand-dependence electronic properties of the studied Ru(II) complexes.
Figure 5 shows the UV–Vis absorption spectra of tbbpy recorded at different irradiation times (10 min–24 h) in acetonitrile. A pronounced overlap of the spectra is observed in the visible region (≈450–500 nm), with no systematic decrease in absorbance intensity over time. This observation is quantitatively supported by the negligible absorbance variations (ΔA% < 3%) and the near-zero apparent rate constants calculated at 484 and 487 nm (Table 3). Consequently, no meaningful photodegradation half-life could be extracted within the experimental timeframe, and the half-life of tbbpy is estimated to be far greater than 24 h.

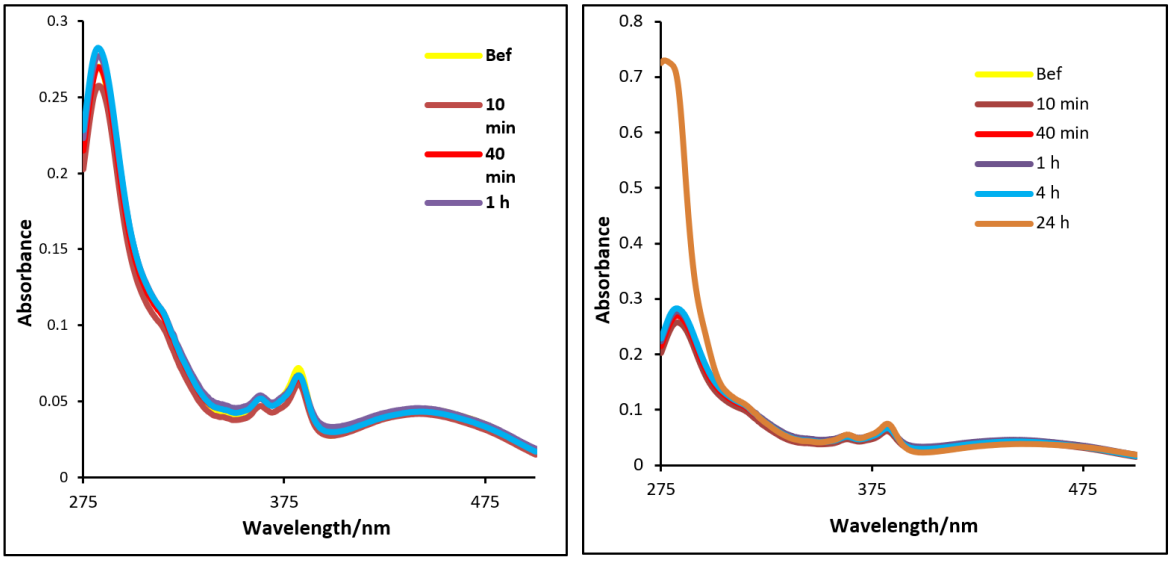

Figure 5. Absorption spectra of $[(tbbpy)_2Ru(tpphz)](PF_6)_2$ at 24^0C in CH_3CN.

In contrast, a significant increase in absorbance is observed in the UV region around 280 nm upon prolonged irradiation (Figure 4). As summarized in Table 3, the absorbance at 280 nm increases by more than 170% after 24 h, which precludes the application of first-order photodegradation kinetics at this wavelength. These changes are therefore attributed to the formation of photogenerated species rather than direct decomposition of the parent compound.

Table 3. UV–Vis absorption bands, time-dependent behavior, and electronic transition assignments of tbbpy in acetonitrile (1×10^{-4} M, 1 cm).

λ (nm)	A_0	$A_{(24h)}$	ΔA%	Time dependence	Assigned electronic transition
280	0.2634	0.7222	+174.2	Strong increase	π → π* (ligand-centered, LC)
383	0.0708	0.0744	+5.1	Slight increase	n → π* / π → π* (ligand-centered)
484	0.0292	0.0293	+0.3	Essentially constant	MLCT (Ru^{2+} → tbbpy)
487	0.0269	0.0275	+2.2	Essentially constant	MLCT (Ru^{2+} → tbbpy)
500	0.0169	0.0196	+15.9	Minor increase	MLCT tail / vibronic band

3.3 Photochemical Kinetics and Stability in Methanol

Time-dependent UV–Vis absorption measurements were carried out in methanol to investigate the photochemical behavior and stability of the Ru(II) complex. The MLCT absorption band exhibited gradual changes in intensity upon irradiation, while the position of the absorption maximum (λ_{max}) remained essentially unchanged over the monitored time interval, suggesting that the dominant process involves absorbance modulation rather than significant spectral shifting as shown in **Figure 6**.

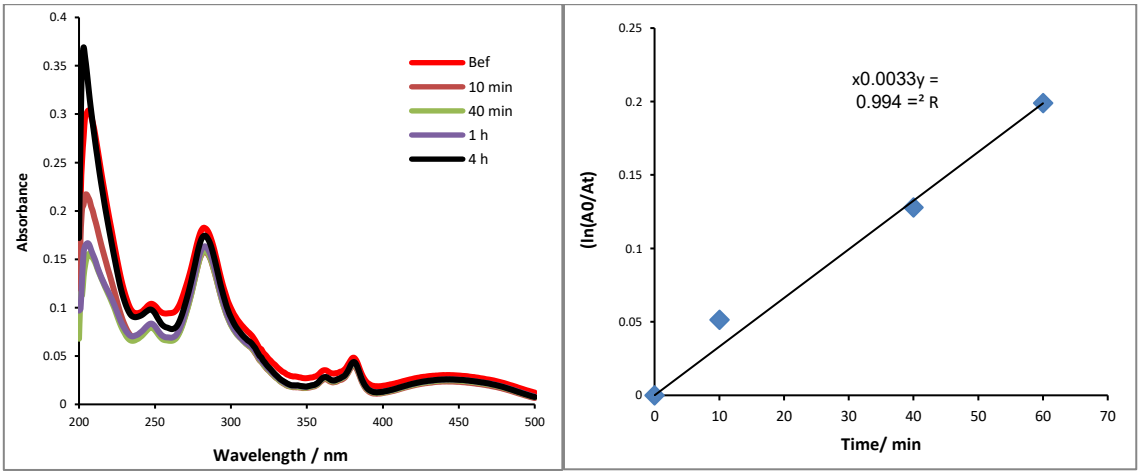

Figure 6: Spectral kinetic study of the photodecomposition of $[(tbbpy)_2Ru(tpphz)](PF_6)_2$ in CH_3OH. (a) Pseudo-first-order kinetic plot showing the linear relationship between $\ln(A_0/A_t)$ and time (min) at 24°C. (b) Time-dependent UV-Vis absorption spectra showing the evolution of absorbance intensity over different time intervals (from 0 to 4 hours).

Kinetic analysis was conducted by tracking the time-dependent changes in the intensity of the MLCT absorption band at λ_{max}. Absorbance values obtained from the UV–Vis spectra (Figure 5(b)) were analyzed under the assumption of pseudo-first-order kinetics. This assumption is supported by the constant irradiation conditions and the large excess of solvent. The plot of $\ln(A_0/A_t)$ versus irradiation time (Figure 5(a)) exhibited a linear correlation, indicating first-order reaction behavior. The proportionality between absorbance and concentration was assumed to follow the Beer–Lambert law.

The photochemical degradation of the complex $(tbbpy)_2Ru(tpphz)_2$ was quantitatively analyzed using a pseudo-first-order kinetic model. The apparent rate constant (k_{app}), obtained from the slope of the linear regression of $\ln(A_0/A_t)$ versus irradiation time within the interval over which linearity was maintained, was determined to be $(3.3 \pm 0.2) \times 10^{-3}$ min^{-1}. The high correlation coefficient ($R^2 = 0.9845$) indicates that the experimental data are well described by the adopted kinetic model under these conditions.

Based on this rate constant, the corresponding half-life ($t_{1/2}$) was calculated using $t_{1/2} = \ln(2)/k_{app}$, yielding a value of (210 ± 13) min (approximately 3.5 h). It should be noted that this half-life is intrinsically linked to the validity of the pseudo-first-order model and is therefore applicable only within the regime where the linear kinetic behavior is observed. The reported uncertainty reflects minor experimental fluctuations and supports the reproducibility of the measurements performed at 24 °C in CH_3OH.

These results indicate that the complex undergoes measurable photo-induced degradation in methanol, displaying moderate photostability under the investigated conditions. This behavior is consistent with the presence of solvent–solute interactions in the protic methanol medium,

3.4 Time – dependent UV- Vis analysis and photostability

To complement the kinetic analysis presented in Section 3.3, the time-dependent UV–Vis spectra of the Ru(II) complex in methanol were recorded and analyzed. These spectra provide insight into the photochemical behavior of the complex under continuous irradiation. As shown in Figure 5, the MLCT bands at 484 and 487 nm remain essentially unchanged over 24 h, indicating notable photostability of the MLCT transitions. In contrast, the high-energy ligand-centered absorption at 280 nm shows a significant increase in absorbance (+85.4%), consistent with $\pi \rightarrow \pi^*$ transitions localized on the ligand framework. Minor variations observed around 500 nm are attributed to vibronic contributions within the MLCT tail rather than to photodegradation.

All measured absorbance values at the MLCT bands, along with the corresponding $\ln(A_0/A_t)$ calculations, are summarized in Table 4, providing a comprehensive record of the temporal evolution of the spectral features. These absorbance trends correlate with the pseudo-first-order kinetics reported in Section 3.3, reinforcing the observation that the Ru(II) complex maintains its structural integrity and excited-state stability in methanol under prolonged irradiation.

Table 4. UV–Vis absorption bands, time-dependent behavior, and electronic transition assignments(1×10^{-4} M, 1 cm, CH_3OH).

λ (nm)	A_0	A (24 h)	ΔA %	Time dependence	Assigned electronic transition
280	0.1781	0.3302	+85.4	Strong increase	$\pi \rightarrow \pi^*$ (ligand-centered, LC)
383	0.0440	0.0467	+6.1	Slight increase	$n \rightarrow \pi^*$ / $\pi \rightarrow \pi^*$ (ligand-centered)
484	0.0199	0.0190	−4.5	Essentially constant	MLCT ($Ru^{2+} \rightarrow$ tbbpy)
487	0.0185	0.0173	−6.5	Essentially constant	MLCT ($Ru^{2+} \rightarrow$ tbbpy)
500	0.0122	0.0105	−13.9	Minor decrease	MLCT tail / vibronic band

4. Discussion

4.1. Structural Influence of Peripheral Ligands on the Electronic Environment

The comparative ^{1}H NMR analysis confirms that peripheral ligand modification induces measurable perturbations in the electronic environment of Ru(II) complexes. The systematically larger downfield shifts observed for the dppz-based complex, particularly for nitrogen-adjacent aromatic protons, reflect enhanced π-delocalization and reduced local electron density. These effects indicate stronger electronic communication between the peripheral ligand and the metal center, supporting the conclusion that such ligands actively modulate metal–ligand interactions rather than acting as passive structural appendages.

4.2. Ligand-Dependent MLCT Energetics

The observed hypsochromic shift and increase in ΔE for the Ru–dppz complex are consistent with stabilization of ligand-centered π* orbitals induced by π-extension. While an increased energy gap is commonly associated with reduced non-radiative decay rates, the present study limits its conclusions to enhanced photochemical robustness rather than direct lifetime extension, as no time-resolved measurements were performed. Nevertheless, the spectral trends strongly suggest that peripheral ligand design can indirectly influence excited-state deactivation pathways.

4.3. Solvent-Mediated Photochemical Pathways

The marked contrast between acetonitrile and methanol highlights the decisive role of solvent–solute interactions. In methanol, the growth of high-energy ligand-centered absorption bands indicates photochemical transformation rather than simple decomposition. Although the exact nature of the photogenerated species remains unresolved, the preservation of MLCT bands confirms retention of the Ru(II) coordination core. These findings emphasize that photostability is governed not solely by ligand electronics but also by solvent accessibility to excited-state relaxation channels.

4.4. Design Implications Rather Than Catalytic Claims

Rather than demonstrating photocatalytic activity directly, this study provides mechanistic insights relevant to photocatalyst design. The ability of π-extended peripheral ligands to modulate MLCT energetics and suppress rapid photodeactivation represents a valuable strategy for developing more robust Ru(II)-based photosensitizers. Future studies integrating time-resolved spectroscopy and catalytic testing will be required to translate these photophysical advantages into functional photocatalytic systems.

Conclusion

This study demonstrates that the stability of the Metal-to-Ligand Charge Transfer (MLCT) state is a direct function of strategic peripheral ligand design. By exploiting the spectral invariance of the Ru–tbbpy complex across both aprotic and protic solvents (where absorption maxima remained identical), we successfully isolated the role of solvent-solute dynamics in photodegradation.

The ^{1}H NMR data confirmed that the π-extended architecture of the dppz ligand does not merely shift the energy gap, but provides a structural "shield" that enhances photochemical resilience compared to the tbbpy analogue. While kinetic analysis identified a clear susceptibility of tbbpy in protic media, the emergence of stable, blue-shifted absorption bands suggests that the process is not a simple decomposition, but rather a photo-induced transformation into new stable species. These findings provide a blueprint for developing more durable Ru(II) sensitizers by tailoring the peripheral ligand environment to suppress non-radiative decay pathways in reactive solvents.

Future work

To further build upon these findings, our future work will focus on identifying the specific photoproducts of Ru-tbbpy degradation using Liquid Chromatography-Mass Spectrometry (LC-MS). Additionally, we aim to employ Femtosecond Transient Absorption Spectroscopy to directly measure the MLCT excited-state lifetimes and explore the fast relaxation dynamics. Finally, computational studies using Density Functional Theory (DFT) will be conducted to model the protective shielding effectnof the dppz ligand at the molecular level, providing a comprehensive framework for designing more resilient photocatalysts.

References

Bolger, J., Gourdon, A., Ishow, E., & Launay, J.-P. (1995). Stepwise syntheses of mono- and di- nuclear ruthenium tpphz complexes $[(bpy)_2Ru(tpphz)]^{-2}$ and $[(bpy)_2Ru(tpphz)Ru(bpy)_2]^{4+}${tpphz=tetrapyrido[3,2-a:2′,3′-c:3″,2″-h:2″,3‴-j]phenazine}. *Journal of the Chemical Society, Chemical Communications*, 1799–1800. https://doi.org/10.1039/C39950001799

Cotic, A., Ramírez-Wierzbecki, I., & Cadranel, A. (2024). Harnessing high-energy MLCT excited states for artificial photosynthesis. *Coordination Chemistry Reviews*, 514, 215878. https://doi.org/10.1016/j.ccr.2024.215878

Di Pietro, M. L., La Ganga, G., Nastasi, F., & Puntoriero, F. (2021). Ru(II)-Dppz Derivatives and Their Interactions with DNA: Thirty Years and Counting. *Applied Sciences*, *11*(7), 3038. https://doi.org/10.3390/app11073038

Fennes, A., Montesdeoca, N., Papadopoulos, Z., & Karges, J. (2024). Rational design of a red-light absorbing ruthenium polypyridine complex as a photosensitizer for photodynamic therapy. *Chemical Communications*,60,10724–10727.
https://doi.org/10.1039/D4CC04126G

Isakov, D., Giereth, R., Nauroozi, D., Tschierlei, S., & Rau, S. (2019). Two emissive long-lived excited states of an imidazole-functionalized ruthenium dipyridophenazine complex. *Inorganic Chemistry*, 58(19), 12646–12653.
https://doi.org/10.1021/acs.inorgchem.9b01372

Khanduja, D., Singh, A., Sharma, P., Gupta, R., Verma, S., & Kumar, V. (2023). Enhanced photostability and photoactivity of ruthenium polypyridyl-based photocatalysts by covalently anchoring onto reduced graphene oxide. *ACS Omega, 8*(15), 13821–13833.
https://doi.org/10.1021/acsomega.3c08800

Kuhnt, C., Karnahl, M., Tschierlei, S., Griebenow, K., Schmitt, M., Schäfer, B., Krieck, S., Görls, H., Rau, S., Dietzek, B., & Popp, J. (2010). Substitution-controlled ultrafast excited-state processes in Ru-dppz-derivatives. *Physical Chemistry Chemical Physics*, 12(6), 1357–1368.
https://doi.org/10.1039/B915770K

Lanquist, A. P., Piechota, E. J., Wickramasinghe, L. D., Marques Silva, A., Thummel, R. P., & Turro, C. (2023). New Tridentate Ligand Affords a Long-Lived 3MLCT Excited State in a Ru(II) Complex: DNA Photocleavage and 1O2 Production. *Inorganic chemistry*, 62(39), 15927–15935.
https://doi.org/10.1021/acs.inorgchem.3c01990

Mohammed, H. A., & Younis, H. A. (2025, November 30). *Investigation of solvent effects on the spectroscopic and photochemical properties of ruthenium(II) polypyridyl complexes* [Paper presentation]. *Proceedings of the Environmental Pollution and Challenges of Environmental Sustainability Conference (EPESC)*. Sirte University Institutional Repository.
http://dspace-su.server.ly:8080/xmlui/handle/123456789/3595

Ruslanova, J., Decurtins, S., Rusanov, E., Stoeckli-Evans, H., Delahaye, S., & Hauser, A. (2002). Ruthenium(II) complex of bis(2,2′-bipyridine)(6,7- dicyanodipyrido[3,2-a:2′,3′-c]phenazine): Synthesis, structure, electrochemical and luminescence studies. *Journal of the Chemical Society, Dalton Transactions*, (23), 4318–4320.
https://doi.org/10.1039/B210440G

Sun, Y., El Ojaimi, M., Hammitt, R., Thummel, R. P., & Turro, C. (2010). Effect of ligands with extended π-system on the photophysical properties of Ru(II) complexes. *The journal of physical chemistry. B*, *114*(45), 14664–14670.
https://doi.org/10.1021/jp102613n

Suneesh, C. V., Balan, B., Ozawa, H., Nakamura, Y., Katayama, T., Muramatsu, M., Nagasawa, Y., Miyasaka, H., & Sakai, K. (2014). Mechanistic studies of photoinduced intramolecular and intermolecular electron transfer processes in RuPt-centred photo-hydrogen-evolving molecular devices. *Physical Chemistry Chemical Physics, 16*(4), 1607–1616.
https://doi.org/10.1039/c3cp54630f

Supporting information

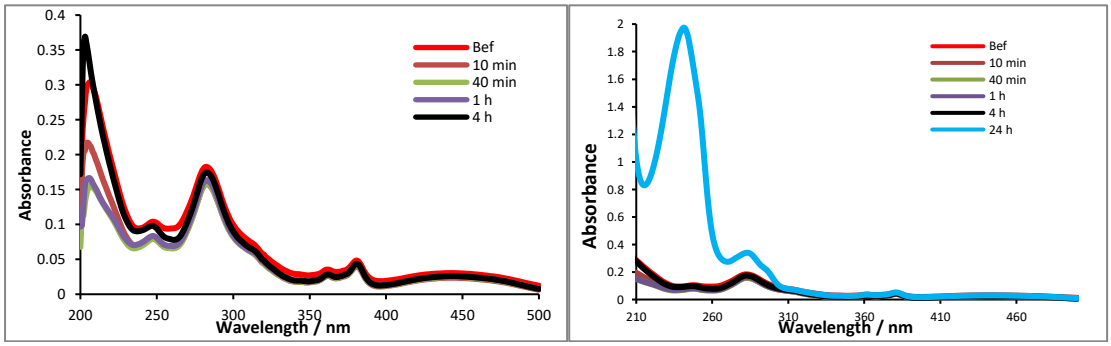

Figure S. Absorption spectra of $[(tbbpy)_2Ru(tpphz)](PF_6)_2$ at 24^0C in CH_3OH

Table L1. Electronic absorption data of ruthenium complexes in different solvents.

Complex (ligand)	Solvent	λ_{abs} (nm)	Assignment	ΔE (eV)
Ru–tbbpy	CH_3CN	201, 282, 382, 446	π→π*, MLCT	2.78
Ru–tbbpy	CH_3OH	207, 284, 381, 446	π→π*, MLCT	2.78
Ru–dppz	CH_3CN	289, 315, 386, 433	π→π*, MLCT	2.86
Ru–dppz	CH_3OH	289, 314, 385, 432	π→π*, MLCT	2.87

Note : ΔE values were estimated from the lowest-energy MLCT absorption maximum using ΔE = 1240/λ.

Table L2: Statistical Parameters and Uncertainty Estimates

Parameter	Value	Uncertainty / Note
Rate Constant(k)	0.0033 min^{-1}	± 0.0002 min^{-1}
Coefficient of Determination (R^2)	0.9845	High reliability
Initial Absorbance Ratio ($\ln(A_o/A_t)$ t=0)	0.0000	Standard reference point
Mean Absolute Error (MAE)	≈0.012	Average deviation from the fit
Maximum Observed Value	1.2039	Recorded at1440 min

Compliance with ethical standards

Disclosure of conflict of interest

The authors declare that they have no conflict of interest.